# Electronic states and metallic character of carbide Co/MoS 2 catalytic interface

Oscar A López-Galán, Manuel Ramos, G. Berhault, Brenda Torres, Russell R Chianelli

# Electronic States and Metallic Character of Carbide Co/$MoS_2$ Catalytic Interface

Oscar A. López-Galán[1], Manuel Ramos[1*], Gilles Berhault[2], Brenda Torres[3] and Russell R. Chianelli[3]

[1]Departamento de Física y Matemáticas, Instituto de Ingeniería y Tecnología, UACJ, 32310 Ciudad Juárez, México.
[2]Institut de Recherches sur la Catalyse et l'Environnement, IRCELYON, CNRS, Université de Lyon, Villeurbanne 69100, France.
[3]Materials Research and Technology Institute, University of Texas at El Paso, El Paso, Texas-USA, 79968.

## Abstract

We report computer assisted density functional theory computations of electronic states in carbide $Co_9S_8/MoS_2$ interface model. The interface model was previously proposed using crystallographic information from experimental high-resolution TEM observations; and directly observed by in-situ heating to confirm carbon deposit occurs at the sulfur edge of $Co_9S_8/MoS_2$ which creates a thin carbide layer. In here, the total energy for carbon adsorption results eight times more favorable to occur at sulfur edge in comparison to molybdenum or cobalt replacement by permutation of carbon atoms as contained in C, CH, $CH_2$ species by exothermic energies. Amorphous carbon excites $2_{pz}$ orbitals as observed on Density of States near $F_E$ level, and 13% decreased in terms of charge carriers available, causing to decrease its chemical catalytic reactivity and $MoS_2$ slabs bending, as carbon starts to accumulate at the sulfur edge, is attributed to charge distribution around the adsorption site caused by the foreign atoms, confirmed by electron density plots, that acts as "electron traps". This helps us concluding that carbon replacement can induce change of selectivity in direct desulfurization pathway (DDS).

**Keywords:** Electronic States, Carbide, $MoS_2$, Catalyst, Energy

Corresponding author: manuel.ramos@uacj.mx

## 1.0 Introduction

As described extensively in the literature, either nickel or cobalt promoted two-dimensional molybdenum disulfide (Co/Ni-[$MoS_2$]) are one of workhorse materials for hydrodesulfurization process [1], with the aim of improving the chemical quality of hydrocarbon-based fuels [2-4]. In order to understand the catalytic mechanism and reactivity extensive studies have been completed during past four decades, concluding $MoS_2$ chemical structure constituted by sandwich-like S=Mo=S bonds ordered in trigonal prismatic with specific packing (*R3m*-hexagonal) analog to other two-dimensional layered materials such as graphene. The chemical bond between stacks (*d*-spacing 0.62 nm) happen due to van der Waals weak forces, making easy to exfoliate, as well to create large array of honeycomb-like superlattice as observed by HRTEM in bulk $MoS_2$ fresh catalyst [5, 6]. It has been extensively proven that promotion made by cobalt or nickel boost $MoS_2$ catalytic activity, due to electron transfer of *d*-orbital as demonstrated by Raybaud *et al.* [7], this promotion effect happens due to Sabatier principle attributed to the *d*-character on transition metal sulfides as proposed by Chianelli *et al.* in periodic trends studies made by density functional theory [8]. Moreover, cobalt sulfide and molybdenum disulfide bulk phases can exist as described extensively by Pavel *et al.* [9] and studies indicate that a direct and indirect metal–metal interactions occur between both phases creating an interface of $Co_9S_8/MoS_2$ [10]. In bulk $Co_9S_8$, cobalt atoms occupy 1/8th of available octahedral sites and half of tetrahedral sites, and layered packing of molybdenum disulfide which can be considered anisotropic material, because (0001)-basal plane is expected to be chemical or catalytic inert due to a fully sulfur coordination, leaving only dangling bonds on (1 0 1 0) and (1 0 1 0) edge planes, which in principle are considered reactive favorable locations for chemical interactions to occur.

When talking about bulk exotic nanostructured morphologies, as described elsewhere when varying chemical synthesis parameters such as temperature, pressure and chemical precursors, some (Co)Ni/$MoS_2$ specific nanorods [7], spheres [11-13], triangular prism [14]. The promoted phase formed by the interaction of cobalt with $MoS_2$ edges was first observed using Mossbauer emission spectroscopy [15] and later by state of art Field Emission Transmission Electron Microscopy (TEM), which enables to achieve direct observations of atomistic positions of cobalt and nickel over layered $MoS_2$ on what it is characteristic fringes as described in the literature when referring to (1 0 1 0) crystallographic plane [16]. Furthermore, computer-imaging simulations by projected potential as described by Stockmann *et al.* had made possible to achieve correlation between experimental and theoretical HRTEM images for $MoS_2$ catalyst [17]. And recently by *Z*-contrast TEM electron tomography as presented by Ramos *et al.* for Co/$MoS_2$ spheres, allowed to describe location and fractal aspects over possible coordination sites within porous of the catalytic particles [18], additionally by using in-situ operando HRTEM it was possible to observe carburization effects due to reactive of fresh Co/$MoS_2$ at temperatures of 350°C to 450°C, which are typical operational temperatures during hydrodesulfurization reactions [19].

As based on experimental evidence reported in previous works about structural and chemical nature related to electronic structure in this computational study, we are presenting the electronic states of carbon permutation on the previously proposed theoretical $Co_9S_8$/$MoS_2$ interface when edge reacts with C, CH, $CH_2$, $CH_3$ and $CH_3SH$ chemical species its correlation to experimental evidence of carburization effects on spent $Co_9S_8$/$MoS_2$ catalyst. Our findings enlighten the nature of $MoS_2$ slabs bending as carbon starts to accumulate at the sulfur edge which, to our best understanding, has remain without plausible explication until now.

## 2.0 Computational Methods

The computer theoretical $MoS_2/Co_9S_8$ model was built using information from high-resolution transmission electron microscopy observations made on fresh $Co_9S_8/MoS_2$ catalyst prepared by hydrothermal methods from ammonium tetrathiomolybdate salt precursors keeping a Co/Mo ratio of 0.3. Detailed description of the hydrothermally obtained $Co_9S_8/MoS_2$ catalyst is reported in prior authors works [10]. Such experimental observations allow us to achieve a complex $Co_9S_8/MoS_2$ interface model in a theoretical form. Due to the complexity of the model, a portion called "*seed*", composed by Sulfur, Cobalt and Molybdenum atoms (37 total) in array such a thiocubane cluster and direct metallic bond between Mo and Co species is our representative of the system (*periodic conditions*) as shown in figure 1a. The geometrical optimization was performed with Broyden–Fletcher–Goldfarb–Shanno quasi-Newtonian algorithm (BFGS) for each carbon deposit process setting a maximum displacement of $2\times10^{-3}$ Å and a convergence threshold for a maximum energy change of $2\times10^{-5}$ eV/atom. Resulted structures were put into a geometrical optimization process. After that, were subjected to total and partial density of states (DOS) calculations with aid of Cambridge Serial Total Energy Package (CASTEP) code [21] as accessible in 9.0 Materials Studio® package, using plane-wave basis (PWB) and cutoff energy set to 300 eV, self-consistent field (SCF) tolerance of $1\times10^{-6}$ eV/atom, and over gamma point only (k-point mesh of 1×1×1) in the Brillouin zone in the reciprocal space. Revised Perdew-Burke-Herzerhof (RPBE) ultrasoft pseudo-potentials, exchange-correlation functional inside the generalized gradient approximation (GGA) were chosen for the electronic description. The model was placed in a non-symmetry ($P_1$) box with dimensions of 20 Å × 20 Å × 20 Å, large enough for avoiding interactions with adjacent cells. The carbon deposits process was proposed such that C, CH, $CH_2$, $CH_3$ and $CH_3SH$ species binds at sulfur-edge, molybdenum-edge and cobalt-edge determining the

corresponding carburization energy (ΔE). It is assumed that the chemical reaction between the carbon species and $Co_9S_8/MoS_2$ seed produces carbide interface and sulfur is released as $H_2S$ product as expressed by equation 1.

$$\Delta E = \left[E(Co_9S_8/MoS_2 + nC) + nE(H_2S) + \left(\frac{1}{2}ny - n\right)E(H_2)\right] - E(Co_9S_8/MoS_2) + nE(CH_y) \quad (1)$$

And for the $CH_3SH$ case, ΔE was calculated according with equation 2.

$$\Delta E = \left[E(Co_9S_8/MoS_2 + nC) + 2nE(H_2S) + \left(\frac{1}{2}ny - n\right)E(H_2)\right] - \left[E(Co_9S_8/MoS_2) + nE((CH_3S)_m) + \frac{1}{2}nE(H_2)\right] \quad (2)$$

Thus, a positive value of ΔE, in both equations, would indicate an endothermic reaction, otherwise implies an exothermic reaction and thus, a thermodynamically more favorable process to occur. The carbon atoms were placed substituting S, Mo and Co at edge sites as indicated in figure 1a, in accordance with experimental observations made during *in-situ* operando HRTEM for carbon deposits near sulfur edge on fresh $Co_9S_8/MoS_2$ catalyst [19] as presented in figure 1b. Furthermore, extensive reports indicate also carburization is thermodynamically favorable to occur near or at surface edges of molecular interfaces [22]. S replacement by C was not considered to take place at the $Co_9S_8$ phase because S disposition would not allow us to study the C-C interaction due the broader localization of S inside the structure. Moreover, $MoS_2$ is the mainly exposed and reactive phase during reactions and thus, the more propense material for carbon to deposit. In general, $Co_9S_8$ acts more as a metallic promoter/support rather than a catalytic material. All geometrical

optimizations were made such that all atoms with exception of those located at central part of *"seed"* can move freely during the calculations to investigate any structural deformation due to carbon deposits.

## 3.0 Results and Discussion

### *3.1 Carburization Energy and Structural Aspects*

The density of states calculations indicates that carbon deposits are more energetically favorable to occur at sulfur edge rather than Mo and Co edge sites by about one eight of its total energy (1/8 $E_T$). From calculations of the electronic states resulted that carburization energies (**ΔE**) have exothermic values, as obtained from $E_T$ values and its usage on equation 1 (SI-1). These values are also displayed in table 1, where it is possible to determine carburization thermodynamic trend as follows C > CH > $CH_2$ > $CH_3$ > $CH_3SH$, in agreement with observations made by Ge *et al.* [22] and Tuxen *et al.* [23]. When carbon atoms integrate at sulfur edge (*as shown in figure 2a*) forms a triple bond, meaning $sp^2$ hybridization by ionic nature to Mo surrounding atoms with similar bond length as for $\alpha$-MoC phase in agreement with previous reports [24-25]; furthermore the ionic bonding was validated by Mulliken charge analysis as listed in table 2 of all atoms surrounding sulfur-carbon sites labelled as $S_1$, $S_2$, $S_3$, $S_4$, $Mo_I$ and $Mo_{II}$ and displayed in figure 2a. Mulliken analysis indicates that carbon species become highly negative with a charge of -0.41|**e**| for $C_1$ and -0.39 |**e**| for $C_2$ while between molybdenum atoms a redistribution of charge occurred, causing all neighbor molybdenum atoms to become more positive in charge values ($Mo_I$ and $Mo_{II}$) as presented in figure 2a, since prior to carbon addition charge values were ~ +0.3|**e**| while after carbon adsorption a value of ~ +0.6|**e**| was found, doubling its initial charge state and charge values; sulfur atoms atop remain almost with the same charge values. The sulfur atoms located at the center of seed, tend to transfer charge from $Mo_I$ and $Mo_{II}$ atoms to $C_1$ and $C_2$ carbon atoms using

142 sulfur atoms as a charge "*bridge*" as explained before by Chiaelli *et al.* [1] and displayed in figure
143 2a. Such charge "*bridge*" corresponds to red electron density clouds where S atoms are located.
144 The later, might indicate that carbon acts as an electron trap rather that an electron promoter, and
145 density of states plots allows to understand about electronic states and its modification due to
146 chemical binding of carbon species on $Co_9S_8/MoS_2$ interface model. The Electron Density
147 Difference (EDD) plots as displayed in figure 2b, where blue color corresponds to electron
148 depletion zone (*donor*) and red color an electron enrichment (*receptor*). The resulting bending of
149 the $MoS_2$ phase could be a direct consequence of the charge promotion, i.e., the two $Co_9S_8$ and
150 $MoS_2$ phases repeal each other due charge difference. The new chemical bonds between Mo-Mo
151 could suggest a metallic contribution in the new electronic structure, the area enclosed as displayed
152 in figure 2c and 2d indicates a charge distribution occurs where carbon was placed at the interface
153 model and it is exemplified by high dense red zones surrounding $C_1$ and $C_2$. The upper zones of
154 $C_1$ and $C_2$ atoms displayed by the blue zone which indicates fewer electrons available at that
155 superficial region, namely, became less reactive, while remaining tightly bonded between them
156 and the surrounding molybdenum atoms ($Mo_I$ and $Mo_{II}$). When it comes to structural terms, a
157 bending of interface upper part towards carbon zones is observed (*figure 2a*) and can be highly
158 attributed to electron charge difference before and after carbon was replaced at sulfur edge, as
159 experimentally observed by *in-situ* operando HRTEM by Ramos *et al.* [19] and previously by
160 Berhault *et al.* [26], as displayed in figure 1b with aid of Synchrotron X-ray diffraction and EELS
161 in order to study carburized process for unsupported molybdenum sulfide catalyst. In here, all
162 bending effect is accompanied by an elongation of almost 20% of bond lengths at central part of
163 interface seed model, i.e., the interface (SI-2). We believe that a partial cause due to carbon
164 deposits, could be attributed to morphology or phase change, as recently presented by Machione

165 *et al.*, indicating that carbon adsorption induced a phase transition between $MoS_2$ 2H to 3R and 1T
166 phases, possibly what is well known as (α)β-$MoS_2$ phase [27]. In table 3, we listed all fractional
167 coordinates for Mo ions, having no replacement by any foreign atoms and $MoS_2$ phase is label
168 from 1 to 6. From here, it was possible to observe some contraction at *z*-direction as estimated by
169 percentual difference before and after carbon geometrical optimization, and at the *x* and *y*
170 coordinate axis Mo ions presents an slight shift to the right side with respect to the initial
171 coordinates, meaning a bending effects in agreement with experimental HRTEM studies [19]. This
172 is confirmed by centroids difference of both cases, as displayed in figure 3 where a superposition
173 of before and after carbon replacement geometrical optimizations help us to illustrate the relative
174 shift of Mo ions having an angle between centroids estimated of 31.98°. Furthermore, before
175 carbon replacement the Mo atoms have a three-fold, six-fold, seven-fold symmetry with octahedral
176 coordination for $Mo_5$, $Mo_3$, $Mo_4$ and $Mo_6$ respectively, excepting $Mo_1$ which conserves its four-
177 fold coordination, the $Mo_{2\text{-}6}$ presented a distinct bonding order after geometrical optimization
178 when carbon replacement takes place. $Mo_5$ goes from a three to a six-folding presenting single
179 Mo-Mo bond, and $Mo_3$ presents one extra bond corresponding to a Mo-Mo interaction as shown
180 in figure 3. The $Mo_4$ ion increases in one its coordination number, going from seven to an
181 octahedral configuration and $Mo_6$ undergoes from octahedral to nine-fold structure and finally the
182 $Mo_2$ increase from four to seven its bond order accompanied with an increase in bond length with
183 its adjacent neighbors. The relevance on coordination number changes might reduce the number
184 of available electrons for conduction/reaction and increase the electron density clouds besides
185 electronic structure near Fermi levels ($E_F$) as estimated by density of states calculations by carbon
186 replacement which is discussed next.

187

### *3.2 Density of States before and after carbon replacement*

In order, to fully understand the electronic structure a series of numerical calculations for density of states (DOS) were performed before and after carbon replacement on $MoS_2/Co_9S_8$ *"seed"* interface model, as reported before [10] with aid of CASTEP© code. Figure 4 presents partial DOS plots which corresponds to *s*, *p*, and *d*-orbitals and total electronic density. This data made possible to observed metallic character near $E_F$ and its perturbation before and after carbon replacement takes place indicated by red dashed circle, a lower metallicity indicates higher selectivity. Furthermore, the presence of Co-Co interactions is said to be responsible of the metallic character due charge transfer to Mo ions as indicated before [10], noteworthy as displayed in figure 5a & 5b partial density states profile when carbon replacement takes place significantly changes the electronic structure near $E_F$ by decreasing about 12% after carbon chemical binds into the structure, this suggesting high selectivity, mainly for direct desulphurization pathway in the HDS operation conditions of fresh molybdenum disulfide catalyst. The carbon $2p_z$ orbitals contribute to *p*-orbital total density by promoting an increase near -5.0 eV, implying carbon orbitals fall below the $1t_{1g}$ level located at the top of the sulfur level group [28]. On other hand the partial metallic *d*-orbitals presents an increase in its electronic states near $E_F$ of around 20% after carbon deposition, even with existence of direct Mo-Mo bonds, which suggest that metallic molybdenum and sulfur *d*-orbitals overlap. From figure 5b it was possible to determine a slight displacement of *p* and *d*-orbitals to more negative values near fermi level, as indicated by black dashed circle. The later can be attributed to sulfur to carbon atoms replacement; considering that highest occupied energy *d*-orbitals contain a sulfur 3*p* component and electrons at $3e_g$ and $2t_{2g}$ antibonding levels could occupied lower energy states, due to carbon replacement as explained extensively by Harris and Chianelli [28, 29]. The observed decrease on total density states at $E_F$ level could be responsible

for lower reactivity of $Co/MoS_2$ catalyst during typical HDS working conditions. Then, the disposition of electrons is expected to diminish near Fermi level, as confirmed by integrating the total DOS from -1.3 to +1.3 eV for both scenarios and verifying a reduction in electronic density cloud around with an estimation of ~16 electrons when no carbon is present on the interface model and to ~14 electrons after carbon is replaced at sulfur edge. This, this represents a decrease of 13% of the available charge carriers able to attract large aromatic molecules during a catalytic cycle, values are presented in table 4. The perturbation occurred at total and partial density of states can be understood by pure geometrical configurations, since after carbon replacement, center of mass for $Co_9S_8/MoS_2$ results filling $d_{yz}$ Mo orbitals near $E_F$ due cobalt metallic contribution, by meaning of periodicity as explained before [30], and it is notable when it is compared to total density of states in same theoretical $MoS_2/Co_9S_8$ interface as reported before [10,31,32, 33].

## 4.0 Conclusions

In here, the electronic states of carbide $MoS_2/Co_9S_8$ interface by meaning of density functional based on experimental observations as reported in previously. The computed density of states shows a significant difference before and after carbon replacement scenarios, with a decrease in density near Fermi level by 12%, due to a shift of total atomic density. Also, a reduction of electronic density cloud with ~16 electrons when no carbon is present and ~14 electrons after carbon is replaced which is a decrease of 13% of charge carriers, indicating an electronic poison effect for the cobalt promoted $MoS_2$ catalytic material. Our density functional theory study indicates that chemical activity, and other parameters can play a role like the tendency to break Mo-S bonds, meaning HDS activity increases at least until a certain level when the metal-sulfur bond strength decreases reaching an optimum for HDS as described by elongation of chemical bonds, on the opposite if the weakening occurs can induce a HDS activity to decrease in agreement

234 with the Sabatier principle. Such phenomena could explain the $MoS_2$ bending as carbon deposits
235 at the edges as observed by HRTEM. Finally, carbon replacement is able to prompt change of
236 selectivity in direct desulfurization pathway (DDS).

237

238 **Acknowledgements**

239 Authors thanks Programa de Fortalecimiento a la Calidad Educativa PFCE-2019 of Secretaria de
240 Eduación Publica of México at Ciudad Universitaria of Universidad Autónoma de Ciudad Juárez
241 for providing with BIOVIA Materials Studio® 9.0 and to Ing. Javier Gamboa and Ing. Javier
242 Tarango for their assistance on the accounts. O. A. L. G. thanks graduate scholarship program of
243 Consejo Nacional de Ciencia y Tecnología-México #735528 and to The Materials Research and
244 Technology Institute of University of Texas at El Paso.

## List of References


[1] R. R. Chianelli, M. Daage, and M. J. Ledoux, “Fundamental Studies of Transition-Metal Sulfide Catalytic Materials,” in Advances in Catalysis, vol. 40, Elsevier, 1994, pp. 177–232.

[2] R. R. Chianelli et al., “Catalytic Properties of Single Layers of Transition Metal Sulfide Catalytic Materials,” Catal. Rev., vol. 48, no. 1, pp. 1–41, Jan. 2006, doi: 10.1080/01614940500439776.

[3] G. Santos, “Road transport and $CO_2$ emissions: What are the challenges?” Transp. Policy, vol. 59, pp. 71–74, Oct. 2017, doi: 10.1016/j.tranpol.2017.06.007.

[4] R. Quadrelli and S. Peterson, “The energy–climate challenge: Recent trends in $CO_2$ emissions from fuel combustion,” Energy Policy, vol. 35, no. 11, pp. 5938–5952, Nov. 2007, doi: 10.1016/j.enpol.2007.07.001.

[5] Russell R. Chianelli, Albert F. Ruppert, Miguel José-Yacamán, ArmandoVázquez-Zavala “HREM studies of layered transition metal sulfide catalytic materials”, Catalysis Today, 23, 3, (1995), 269-281.

[6] Manuel A. Ramos, Russell Chianelli, Jose Luis Enriquez-Carrejo, Gabriel A. Gonzalez, Gilles Berhault, “Metallic states by angular dependence in 2H-$MoS_2$ slabs”, Computational Materials Science, 84, (2014), 18–22.

[7] H. Toulhoat, P. Raybaud, S. Kasztelan, G. Kresse, J. Hafner, “Transition metals to sulfur binding energies relationship to catalytic activities in HDS: back to Sabatier with first principle calculations”, Catalysis Today, 50, (3-4), 629-636.

[8] R. R. Chianelli, G. Berhault, P. Raybaud, S Kasztelan, J Hafner, H Toulhoat, “Periodic trends in hydrodesulfurization: in support of the Sabatier principle”, Applied Catalysis A: General 227 (1-2), 83-96.

[9] A. Hadj-Aïssa, F. Dassenoy, C. Geantet and P. Afanasiev, “Solution synthesis of core–shell $Co_9S_8$@$MoS_2$ catalysts”, Catal. Sci. Technol., 2016, (6), 4901-4909.

[10] M. Ramos, G. Berhault, D. A. Ferrer, B. Torres, R. R. Chianelli, “HRTEM and molecular modeling of the $MoS_2$–$Co_9S_8$ interface: understanding the promotion effect in bulk HDS catalysts”, Cat. Sci. & Tech., 2, (1), 164-178.

[11] X. Zheng, “Ultrasound-assisted cracking process to prepare $MoS_2$ nanorods,” Ultrason. Sonochem., vol. 11, no. 2, pp. 83–88, Apr. 2004, doi: 10.1016/S1350-4177(03)00137-8.

[12] M. Z. Saidi et al., “Effect of morphology and hydrophobization of $MoS_2$ microparticles on the stability of poly-α-olefins lubricants,” Colloids Surf. Physicochem. Eng. Asp., vol. 572, pp. 174–181, Jul. 2019, doi: 10.1016/j.colsurfa.2019.04.003.

[13] H. Shi, X. Fu, X. Zhou, D. Wang, and Z. Hu, “A low-temperature extraction–solvothermal route to the fabrication of micro-sized $MoS_2$ spheres modified by Cyanex 301,” J. Solid State Chem., vol. 179, no. 6, pp. 1690–1697, Jun. 2006, doi: 10.1016/j.jssc.2006.02.030.

[14] J. Lauritsen et al., “Location and coordination of promoter atoms in Co- and Ni-promoted MoS2-based hydrotreating catalysts,” J. Catal., vol. 249, no. 2, pp. 220–233, Jul. 2007, doi: 10.1016/j.jcat.2007.04.013.

[15] H. Topsoe, “In situ Mossbauer emission spectroscopy studies of unsupported and supported sulfided Co-Mo hydrodesulfurization catalysts: Evidence for and nature of a Co-Mo-S phase,” J. Catal., vol. 68, no. 2, pp. 433–452, Apr. 1981, doi: 10.1016/0021-9517(81)90114-7.

[16] A. Vázquez, “High resolution electron microscopy of $MoS_2$: Ni, $MoS_2$: Co and $MoS_2$: Fe layered crystals,” Mater. Lett., vol. 35, no. 1–2, pp. 22–27, Apr. 1998, doi: 10.1016/S0167-577X(97)00224-3.

[17] R. M. Stockmann, H. W. Zandbergen, A. D. van Langeveld, and J. A. Moulijn, “Investigation of $MoS_2$ on $\gamma$-$Al_2O_3$ by HREM with atomic resolution,” J. Mol. Catal. Chem., vol. 102, no. 3, pp. 147–161, Oct. 1995, doi: 10.1016/1381-1169(95)00111-5.

[18] M. Ramos, F. Galindo-Hernández, I. Arslan, T. Sanders, J. M. Domínguez. “Electron tomography and fractal aspects of $MoS_2$ and $MoS_2$/Co spheres”, Scientific Reports, 7 (1), (2017), 1-9.

[19] Manuel Ramos, Domingo Ferrer, Eduan Martinez-Soto, Hugo Lopez-Lippmann, Brenda Torres, Gilles Berhault and Russell R Chianelli, “In-situ HRTEM study of the reactive carbide phase of Co/$MoS_2$ catalyst” Ultramicroscopy, 127, (2013), 64–69. doi: 10.1016/j.ultramic.2012.07.012.

[20] G. A. Gonzalez, M. Alvarado, M. A. Ramos, G. Berhault, and R. R. Chianelli, “Transition states energies for catalytic hydrodesulfurization reaction in $Co_9S_8$/$MoS_2$ theoretical interface using computer-assisted simulations,” Comput. Mater. Sci., 121, 240–247, (2016), doi: 10.1016/j.commatsci.2016.04.011.

[21] S. J. Clark et al., First principles methods using CASTEP, Z. Für Krist. - Cryst. Mater., vol. 220, no. 5/6, Jan. 2005, doi: 10.1524/zkri.220.5.567.65075.

[22] H. Ge *et al.*, Carbonization of Ethylenediamine Coimpregnated CoMo/$Al_2O_3$ Catalysts Sulfided by Organic Sulfiding Agent, ACS Catal., Vol. 4, 8, 2556–2565, (2014), doi: 10.1021/cs500477x.

[23] A. Tuxen et al., “An atomic-scale investigation of carbon in $MoS_2$ hydrotreating catalysts sulfided by organosulfur compounds,” J. Catal., vol. 281, no. 2, pp. 345–351, Jul. 2011, doi: 10.1016/j.jcat.2011.05.018.

[24] J. R. dos S. Politi, F. Viñes, J. A. Rodriguez, and F. Illas, “Atomic and electronic structure of molybdenum carbide phases: bulk and low Miller-index surfaces,” Phys. Chem. Chem. Phys., vol. 15, no. 30, p. 12617, 2013, doi: 10.1039/c3cp51389k.

[25] P. Liu and J. A. Rodriguez, “Catalytic Properties of Molybdenum Carbide, Nitride and Phosphide: A Theoretical Study,” Catal. Lett., vol. 91, no. 3/4, pp. 247–252, Dec. 2003, doi: 10.1023/B:CATL.0000007163.01772.19.

[26] G. Berhault *et al.*, “The Role of Structural Carbon in Transition Metal Sulfides Hydrotreating Catalysts,” J. Catal., vol. 198, no. 1, pp. 9–19, Feb. 2001, doi: 10.1006/jcat.2000.3124.

[27] M. A. Macchione *et al.*, “Electron microscopy study of the carbon-induced 2H–3R–1T phase transition of $MoS_2$,” New J. Chem., vol. 44, no. 4, pp. 1190–1193, 2020, doi: 10.1039/C9NJ03850G.

[28] S. Harris, “Catalysis by transition metal sulfides: A theoretical and experimental study of the relation between the synergic systems and the binary transition metal sulfides,” J. Catal., vol. 98, no. 1, pp. 17–31, Mar. 1986, doi: 10.1016/0021-9517(86)90292-7.

[29] S. Harris, “Catalysis by transition metal sulfides: The relation between calculated electronic trends and HDS activity,” J. Catal., vol. 86, no. 2, pp. 400–412, Apr. 1984, doi: 10.1016/0021-9517(84)90385-3.

[30] R. R. Chianelli, G. Berhault, P. Raybaud, S. Kasztelan, J. Hafner, and H. Toulhoat, “Periodic trends in hydrodesulfurization: in support of the Sabatier principle,” Appl. Catal. Gen., vol. 227, no. 1–2, pp. 83–96, Mar. 2002, doi: 10.1016/S0926-860X(01)00924-3.

[31] Francoise Maugé, Jean Francois Paul, Laetitia Oliviero, Luz Zavala Sanchez and Ibrahim Khalil, “Structure and quantification of edge sites of $WS_2/Al_2O_3$ catalysts coupling IR/CO spectroscopy and DFT calculations” ChemCatChem 10.1002/cctc.201902053

[32] Ibrahim Saana Amiinu, Zonghua Pu, Daping He, Hellen Gabriela Rivera Monestel, Shichun Mu, “Scalable cellulose-sponsored functionalized carbon nanorods induced by cobalt for efficient overall water splitting” Carbon, Volume 137, Oct.2018, doi: 10.1016/j.carbon.2018.05.025.

[33] Hanwen Xu et al. “Two-Dimensional $MoS_2$: Structural Properties, Synthesis Methods, and Regulation Strategies toward Oxygen Reduction”, Micromachines 2021, 12(3), 240; https://doi.org/10.3390/mi12030240

## List of Tables

**Table 1.** Calculated change in energy (**ΔE**) before and after for carbon replacement at sulfur edge using different carbonic agents.

| *Carbon source* | Carbon at Sulfur edge (eV/atom) (*this work*) | Carbon at Sulfur edge (eV/atom) (*ref* [22]) |
|---|---|---|
| ***C*** | -1.55 | -5.27 |
| ***CH*** | -1.43 | -4.03 |
| ***$CH_2$*** | -1.30 | -2.36 |
| ***$CH_3$*** | -1.16 | 1.06 |
| ***$CH_3SH$*** | -0.17 | 1.21 |

**Table 2.** Mulliken analysis of charge distribution of all species around the site.

| ***Atoms*** | **Charge (Before) \|e\|** | **Charge (After) \|e\|** |
|---|---|---|
| $C_1$ | - | -0.41 |
| $C_2$ | - | -0.39 |
| $S_1$ | -0.21 | -0.25 |
| $S_2$ | -0.25 | -0.21 |
| $S_3$ | -0.16 | -0.05 |
| $S_4$ | -0.01 | -0.08 |
| $Mo_I$ | +0.36 | +0.61 |
| $Mo_{II}$ | +0.23 | +0.56 |

**Table 3.** Fractional coordinates and calculated centroid values with its relative change before and after carbon replacement at sulfur edge.

| | **No carbon** | | | **Carbon at sulfur edge** | | | | | |
|---|---|---|---|---|---|---|---|---|---|
| ***Ion*** | **x** | **y** | **z** | **x** | **y** | **z** | **Δx %** | **Δy %** | **Δz %** |
| ***Mo₁*** | 0.4449 | 0.6660 | 0.4895 | 0.4808 | 0.6872 | 0.4807 | 7.4627 | 3.0763 | -1.8283 |
| ***Mo₂*** | 0.3307 | 0.5547 | 0.5167 | 0.3545 | 0.5340 | 0.4946 | 6.7034 | -3.8646 | -4.4553 |
| ***Mo₃*** | 0.5940 | 0.6224 | 0.4766 | 0.6052 | 0.6486 | 0.4850 | 1.8623 | 4.0378 | 1.7314 |
| ***Mo₄*** | 0.4815 | 0.5139 | 0.5036 | 0.4880 | 0.5500 | 0.4809 | 1.3349 | 6.5706 | -4.7102 |
| ***Mo₅*** | 0.7454 | 0.5784 | 0.4637 | 0.7343 | 0.5781 | 0.4426 | -1.5106 | -0.0581 | -4.7656 |
| ***Mo₆*** | 0.6331 | 0.4700 | 0.4906 | 0.6282 | 0.5086 | 0.4676 | -0.7798 | 7.6003 | -4.9291 |
| ***Centroid*** | **0.5204** | **0.5638** | **0.4898** | **0.5341** | **0.5811** | **0.4749** | **2.5733** | **2.9712** | **-3.1303** |

**Table 4.** Estimated values of density of states integration near Fermi level.

| ***Situation*** | **Number of electrons** |
|---|---|
| *Without carbon replacement* | 15.73 |
| *With Carbon replacement* | 13.97 |

# List of Figures

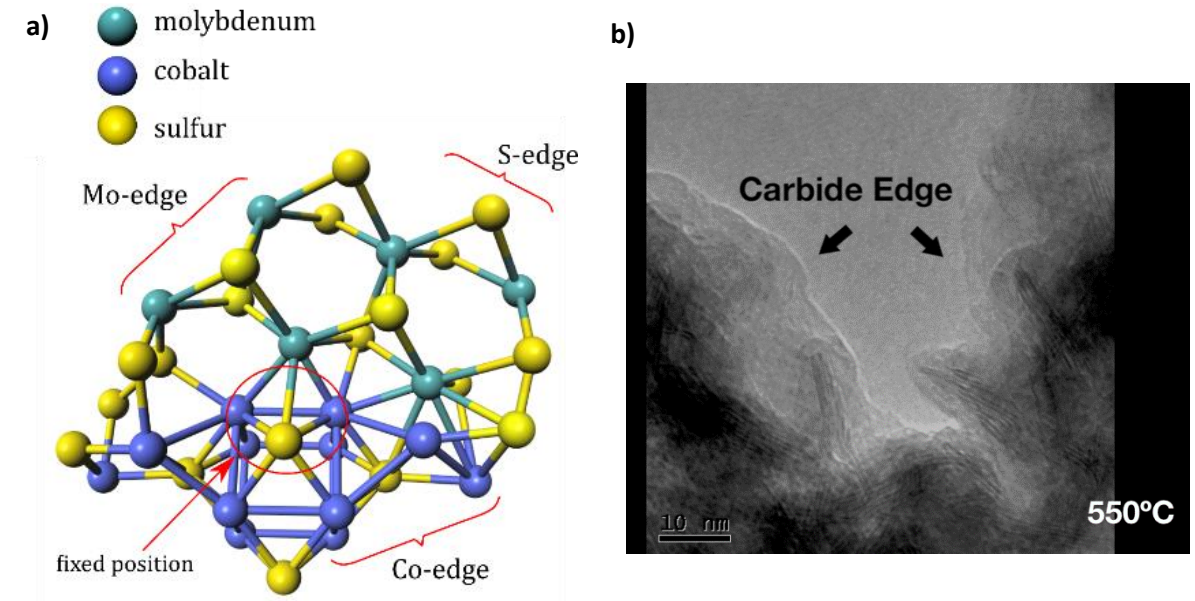


(Color code: Yellow atoms: Sulfur, Blue: Cobalt, Green Aqua: Molybdenum)

**Figure 1.** a) The $Co_9S_8/MoS_2$ interface called "seed" used to perform all Density of States and electronic structure calculations, with sites where carbon was replaced. b) Experimental high-resolution transmission electron microscopy image taken during carburization procedure by in-situ operando heating at 550°C using a Gatan® holder, where is possible to observe the carburization process taking place as indicate by inset labels. [Image adapted with copyrights and permissions from ELSEVIER© Ultramicroscopy, 127, (2013), 64–69.]

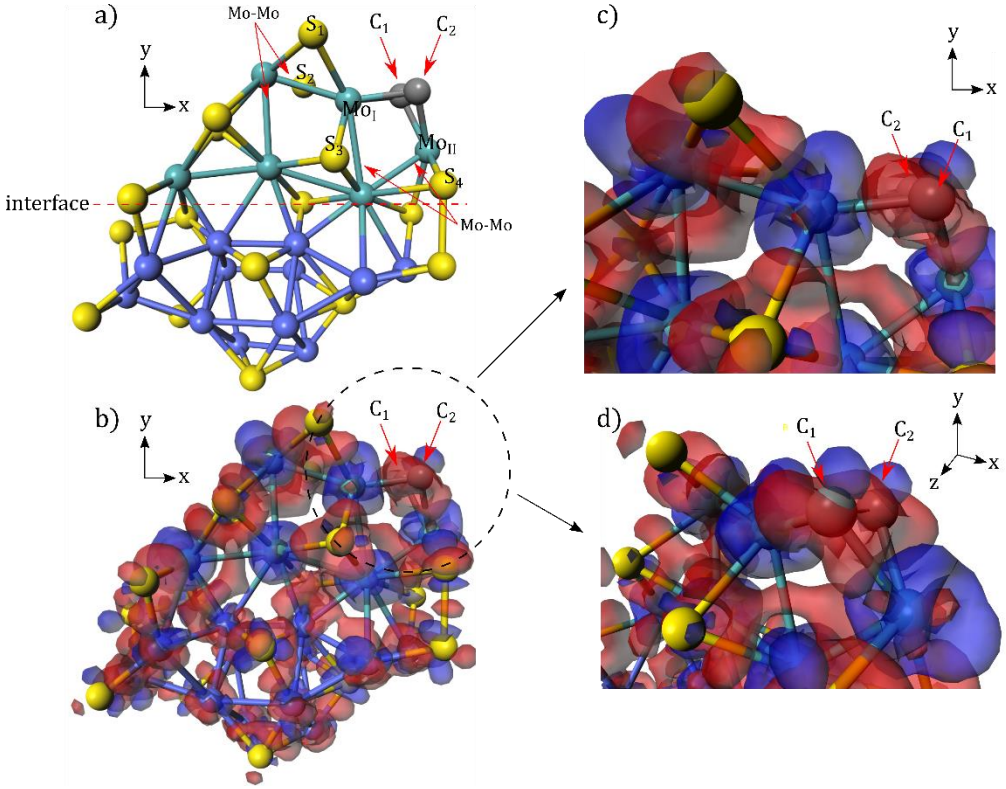


**Figure 2.** a) Geometrical optimized $Co_9S_8/MoS_2$ interface with carbon replacement at sulfur edge. b) Resulting electron difference of the interface. c) Zoom of the encircle area in b). d) zoomed and rotated area around the carbon deposit at sulfur edge. It can be observed the dense red zone surrounding both carbon atoms.

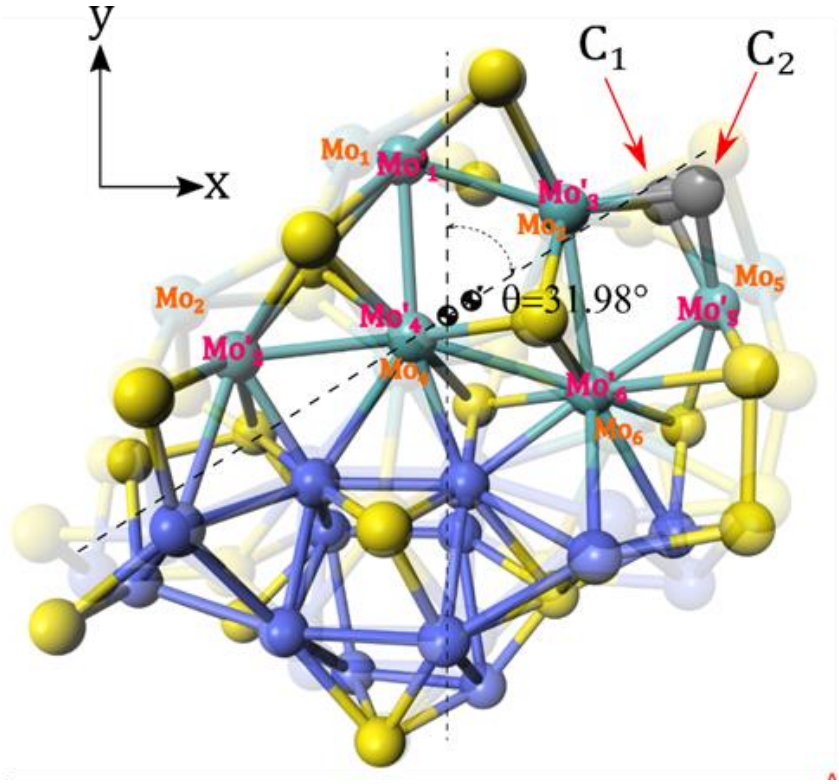


**Figure 3.** Structural comparison on interface seed model before and after carbon replacement. Solid-colored atoms resemble the interface with carbon. The centroid symbol with the apostrophe corresponds to carbon-at-the sulfur-edge. (Color code: Yellow atoms: Sulfur, Blue: Cobalt, Green Aqua: Molybdenum, Black: Carbon)

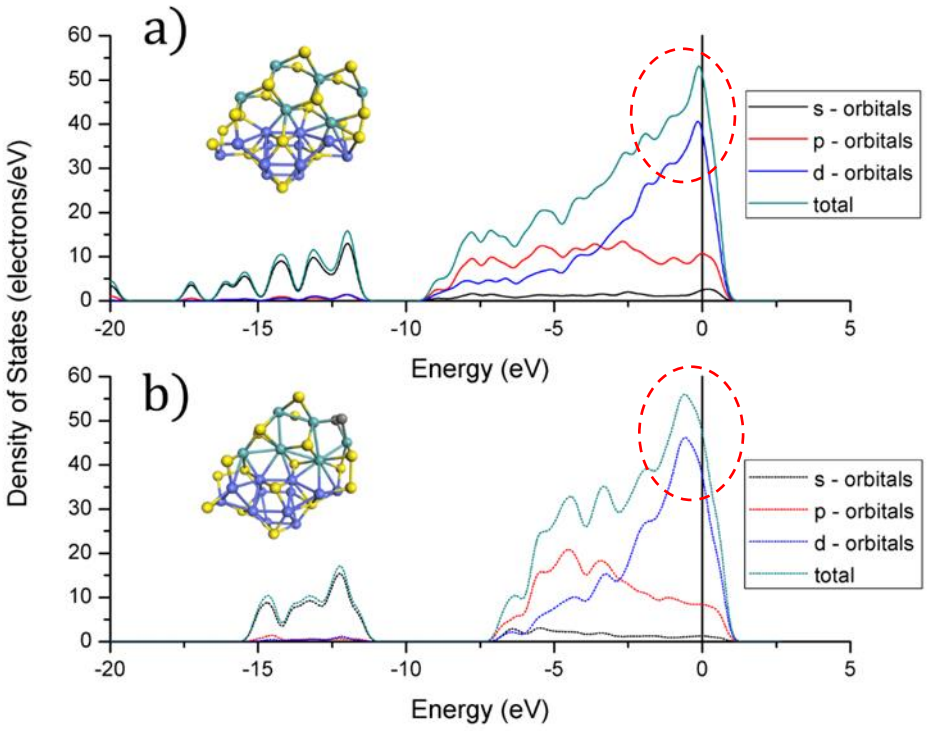


**Figure 4.** Total and Partial Density of States calculated for the $Co_9S_8/MoS_2$ interface before and after carbon replacement, dashed red circles indicates a perturbation of metallic states before and after near $E_F$. (Insets: Optimized seed interface before and after carbon deposition).

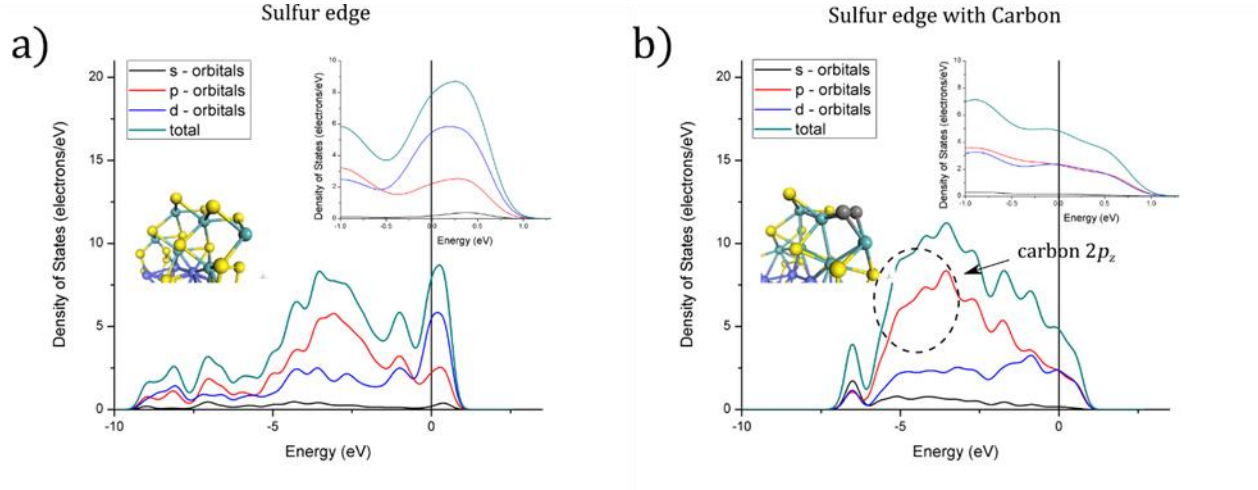


**Figure 5.** a) Partial Density of States before carbon deposit. b) Partial Density of States after carbon deposition. Insets: Enlarged area at the vicinity near Fermi level.

Supplementary information

*S1.* **ΔE** calculations

| **Long name** | **Initial Energy** | **Final Energy** | | | |
|---|---|---|---|---|---|
| | **(Crystal Seed)** | **[Carbon substituting S (S-site)]** | **ΔE** | **ΔE/n** | **ΔE/n** |
| **Units** | **(eV)** | **(eV)** | **(eV)** | **(eV/atom)** | **(kcal/mol)** |
| | -29370.62 | -29154.27 | 508.24 | 13.74 | 316.76 |
| | | **Carbon substituting Mo (Mo-site)** | | | |
| | | | | | |
| | | -25830.79 | 3831.71 | 103.56 | 2206.22 |
| | | **Carbon substituting Co (Co-site)** | | | |
| | | | | | |
| | | -27622.01 | 2040.49 | 55.15 | 1089.83 |
| **n= (# atoms)** | **37** | | | | |
| | **Carbon (Energy calculation)** | | | | |
| | **(eV)** | | | | |
| | -145.94 | | | | |

*S2. Bond distance change*

Bonds between the $MoS_2$ phase and $Co_9S_8$ increased approximately a 20% with respect to the no carbon case.

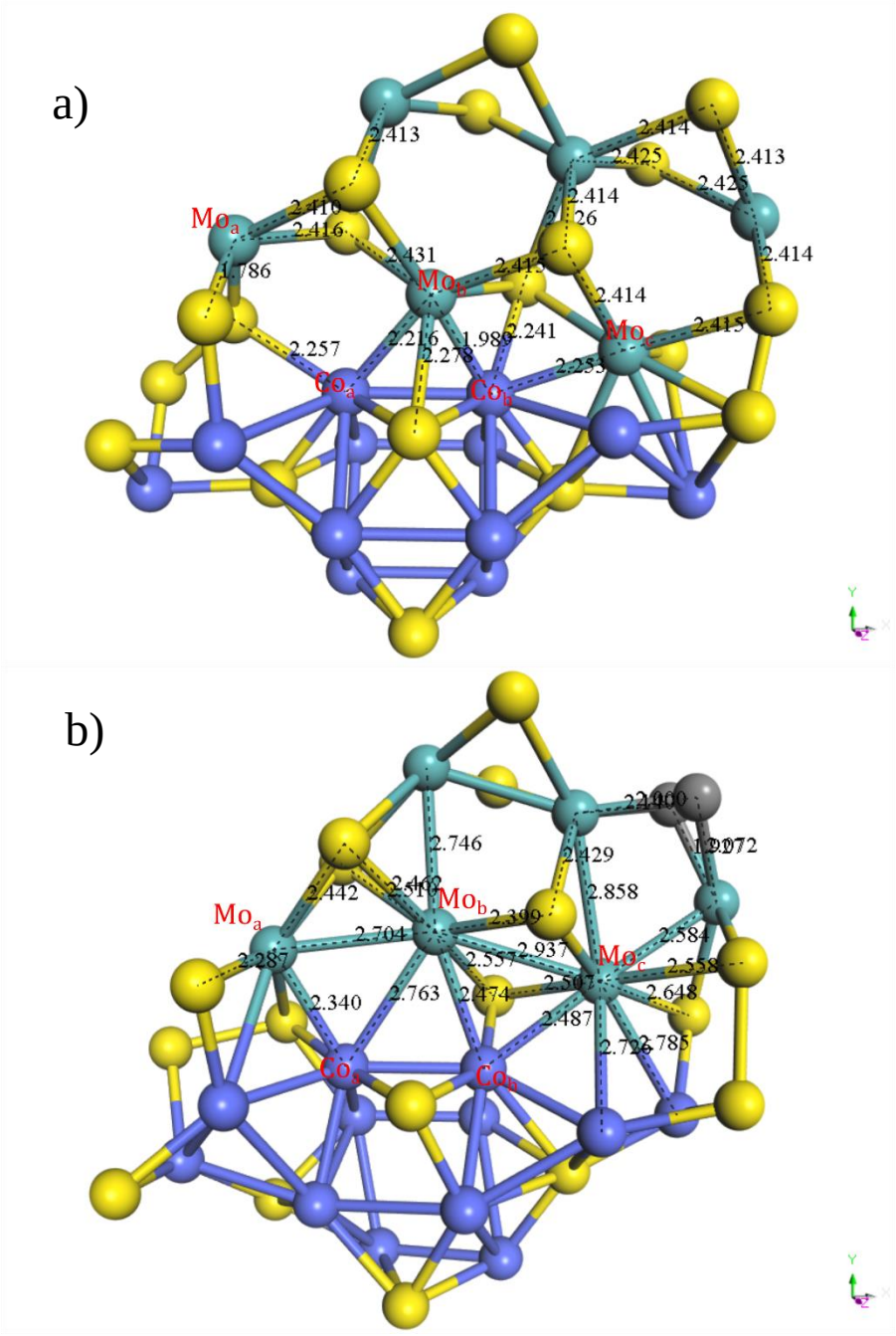


SFigure 1. a) Interface without carbon and b) interface with carbon. Units are in Å. $Mo_a$ change their bond length with neighbor sulfur atoms from 1.786 and 2.416 Å to 2.287 and 2.442 Å with an increase of 22% and 1%, respectively. Bonding between $Co_a$ and $Mo_b$ change from 2.216 to 2.763 Å, representing an increase of 22%.